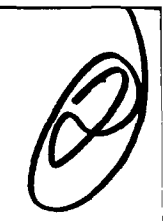

OFFICE OF NAVAL RESEARCH

Grant # N0001489J1848

R&T Code 413u002

Technical Report No. 8

Nucleation and growth of diamond on carbon-implanted single crystal copper

by

T.P. Ong, F. Xiong, R.P.H. Chang, and C.W. White

prepared for publication in the

Journal of Materials Research

Northwestern University
Dept. of Materials Science and Engineering,
Evanston, IL 60208

April 1992

REPORT DOCUMENTATION PAGE

Form Approved
OMB No. 0704-0188

1. AGENCY USE ONLY (Leave blank)	2. REPORT DATE	3. REPORT TYPE AND DATES COVERED
	1992	Technical

4. TITLE AND SUBTITLE
Nucleation and Growth of Diamond on Carbon-Implanted Single Crystal Copper

5. FUNDING NUMBERS
G N0001489J1848
R&T code 413u002

6. AUTHOR(S)
T.P. Ong, F. Xiong, R.P.H. Chang, and C.W. White

7. PERFORMING ORGANIZATION NAME(S) AND ADDRESS(ES)
Materials Science & Engineering Dept.
Northwestern University
2225 Sheridan Road
Evanston, IL 60208

8. PERFORMING ORGANIZATION REPORT NUMBER
Technical Report #8

9. SPONSORING/MONITORING AGENCY NAME(S) AND ADDRESS(ES)
Chemistry Division
Office of Naval Research
800 N. Quincy Street
Arlington, VA 22217-5000

10. SPONSORING/MONITORING AGENCY REPORT NUMBER

11. SUPPLEMENTARY NOTES

12a. DISTRIBUTION/AVAILABILITY STATEMENT
This document has been approved for public release and sale; its distribution is unlimited

12b. DISTRIBUTION CODE

13. ABSTRACT *(Maximum 200 words)*

The nucleation and growth of diamond crystals on single crystal copper surfaces has been studied. Microwave plasma enhanced chemical vapor deposition (MPECVD) was used for diamond nucleation and growth. Prior to diamond nucleation, the single crystal copper surface is modified by carbon ion implantation at an elevated temperature (~820 °C) . This procedure leads to the formation of a graphite film on the copper surface, resulting in the great enhancement of diamond crystallite nucleation. A simple lattice model has been constructed to describe the mechanism of diamond nucleation on graphite as $\langle 111 \rangle_{diamond}$ parallel to $\langle 0001 \rangle_{graphite}$ and $\langle 110 \rangle_{diamond}$ parallel to $\langle 1120 \rangle_{graphite}$. This leads to a good understanding of diamond growth on carbon-implanted copper surfaces.

14. SUBJECT TERMS
Nucleation; diamond growth mechanism; carbon-implanted; copper crystals

15. NUMBER OF PAGES
40

16. PRICE CODE

17. SECURITY CLASSIFICATION OF REPORT	18. SECURITY CLASSIFICATION OF THIS PAGE	19. SECURITY CLASSIFICATION OF ABSTRACT	20. LIMITATION OF ABSTRACT
UNCLASSIFIED	UNCLASSIFIED	UNCLASSIFIED	UL

Nucleation and Growth of Diamond on Carbon-Implanted Single Crystal Copper

T. P. Ong,[a] Fulin Xiong, and R. P. H. Chang
Department of Materials Science and Engineering, Northwestern University, Evanston, IL 60208

C. W. White
Solid State Division, Oak Ridge National Laboratory, Oak Ridge, TN 37831

ABSTRACT

The nucleation and growth of diamond crystals on single crystal copper surfaces has been studied. Microwave plasma enhanced chemical vapor deposition (MPECVD) was used for diamond nucleation and growth. Prior to diamond nucleation, the single crystal copper surface is modified by carbon ion implantation at an elevated temperature (~820 °C) . This procedure leads to the formation of a graphite film on the copper surface, resulting in an enhancement of diamond crystallite nucleation. A simple lattice model has been constructed to describe the mechanism of diamond nucleation on graphite as <111>diamond parallel to <0001>graphite and <110> diamond parallel to $<11\bar{2}0>$graphite. This leads to a good understanding of diamond growth on carbon-implanted copper surfaces.

a)Present address : Jet Propulsion Laboratory, California Institute of Technology, 4800 Oak Grove Drive, M/S 303-308, Pasadena, CA 91109-8099

I. INTRODUCTION

The unique properties of diamond make it one of the most desirable materials for high power electronic devices.[1] However, the technology of high quality single crystal diamond film growth thus far is limited to homoepitaxy.[2] One reason for this limitation is that diamond nucleation on non-diamond substrates is very difficult due to the extremely high surface energy of diamond.[3] An attempt to grow epitaxial diamond film on a single crystal Ni substrate has met little success.[4] The explanation is that nickel preferentially turns the carbon gas species into soot or graphitic carbon.[5,6] Koizumi et. al.[7] reported that diamond can be grown heteroepitaxially on a single crystal c-BN substrate (lattice constant a = 3.616 Å vs. $a_{diamond}$ = 3.5671 Å). However, a large single crystal of c-BN is even harder to come by than diamond itself. The largest c-BN crystal that can be synthesized so far is only 100 μm. Copper (a = 3.6148 Å) is the next best candidate for the substrate, due to its small lattice mismatch with diamond and low carbon solubility precluding the possibility of carbide formation.

Like most other materials, the surface energy of copper is very small, compared to that of diamond ($\gamma_{Cu(100)} = 2.08\ J/m^2$; $\gamma_{diamond(100)} \sim 9.2\ J/m^2$).[3,8] A very interesting initial study of using the copper crystals as substrates for diamond growth is to modify the surface energy of the copper to enhance diamond nucleation. This increase in surface energy is accomplished by carbon ion implantation prior to diamond growth. In this paper, the study of the nucleation and growth of diamond on modified surfaces of single crystal Cu (100) and Cu(111) is presented, and a model to explain diamond growth on ion-implanted copper surface is proposed.

II. EXPERIMENTAL

Copper shot (99.999% pure) was utilized to produce the single crystal copper boule using the Bridgman technique. Sample pieces in a size of about 10x10x1 mm^3 were sliced from the boule along (100) or (111) crystal orientations. Carbon ion implantation was carried out in a vacuum at temperatures in the range of 25 °C to 840 °C with the beam energy in the range from 65 keV to 120 keV. A dose of $1x10^{18}$ ions/cm^2 was used for all samples.

Microwave plasma-enhanced chemical vapor deposition (MPECVD) for diamond growth was carried out using a tubular microwave plasma reactor, as shown in Figure 1. The discharge was maintained by a 1 kW microwave generator operating at 2.45 GHz. A quartz reactor of 25 mm diameter and 830 mm length was placed inside a water-cooled microwave cavity. Gas flow rates were controlled by mass flow controllers and the pressure maintained at a deposition pressure by a by-pass valve installed between the chamber and the mechanical pump.Temperature measurement used a type-K thermocouple with the thermocouple junction positioned just beneath the graphite substrate and shielded by a quartz tube (diameter= 6 mm). The typical deposition conditions were : Flow rates: 3% CH_4 or 0.5% CH_4 and 0.7% O_2 in 200 sccm H_2; Pressure: 33 Torr; Temperature: 800 °C; and Microwave power: 340 W.

A variety of analytic techniques were employed to characterize both carbon-implanted and subsequently diamond-grown samples. The first category of the analytical techniques included high energy (2 MeV) ion Rutherford backscatering

spectroscopy (RBS) and ion channeling measurements, x-ray diffraction analysis, and Raman spectroscopy. They were used to determine the crystal structure and composition of the copper substrate and diamond crystallites. The second class of analytical measurements included various microscopy techniques, such as scanning electron microscopy (SEM), transmission electron microscopy (TEM), scanning tunneling microscopy (STM) and atomic force microscopy (AFM). They were used to elucidate the structural relationship between the substrate and the crystallites. .

III. RESULTS AND DISCUSSION

A. Microstructure of implanted carbon

Generally speaking, during implantation, energetic ions penetrate the target surface and are stopped inside the target, resulting lattice damage in the near surface region of the target. However, in the case of carbon ion implantation into a copper substrate, different results can be obtained depending on the implantation conditions. It should be noted that carbon solubility in copper is very small and no carbide can be formed. In the case of room temperature implantation of carbon into copper crystals, the carbon atoms are embedded to a depth of ~1500 Å for an ion energy of 125 keV. During subsequent thermal annealing at elevated temperature (~800 °C), the embedded carbon atoms diffuse to the surface and form a graphite layer. If ion implantation is carried out at an elevated substrate temperature (~800 °C) implanted carbon atoms diffuse to the surface during implantation, resulting in graphite film formation during the implantation process. Figure 2 shows an optical micrograph of a carbon layer on a carbon-implanted Cu (100) crystal at the following conditions: substrate temperature of 820 °C, a dose of $1x10^{18}$ ions/cm^2, and the beam energy of 70 keV. Carbon islands of a size of approximately 20-30

μm are clearly observed on the surface of the substrate. The thickness of the carbon layer is estimated to be about 900 Å (thickness = ion dose / graphite density). Figure 3 shows RBS and ion channeling spectra taken from this sample. The experiment was performed with 2 MeV He ions at a scattering angle of 160°. Following implantation at elevated temperature (Fig. 3) we observed that leading edge of the random spectrum and the surface peak of the aligned spectrum are both shifted to lower energies relative to spectra taken on an unimplanted (virgin) part of the crystal.This energy shift is due to the presence of a 900 Å carbon layer on the surface following implantation. It is also interesting to note that the channeling yield following implantation is only slightly greater than that in the virgin sample. This shows that implantation at a temperature of ~820 °C introducs very few extended defects in the near surface region.

Figure 4 shows the RBS and channeling analysis following implantation at room temperature for the same beam energy and dose. In this case, carbon is embedded in the near surface region with a maximum in the distribution at a depth of ~800 Å (Fig. 4). The channeling yield in the implanted region is quite high following room temperature implantation. This shows that substantial lattice disorder is produced in the near surface by room temperature implantation, althpough but the near surface remains crystalline and has not turned amorphous by this implantation.

X-ray diffraction analysis of a Cu(111) sample implanted with carbon ions at 820 °C (see Figure 5) shows that the top layer consists of graphite with c-axis of the hexagonal graphite lattice perpendicular to the Cu(111) surface. The (0002) reflection of the graphite (θ=12.84° with detector fixed at 26.54°) is found to be

misoriented within 0.5° with respect to the Cu (111) reflection. This finding is similarly found in the case of Cu(100) substrate. The $d_{(0002)}$ spacing is calculated to be 3.356 Å which is in good agreement with the theoretical value of 3.354 Å.

Transmission electron microscopy (TEM) analysis further confirms the highly oriented graphitic structure of the top layer. A plane view specimen from a Cu(111) sample implanted at high temperature is prepared by chemically etching the Cu substrate away and then the graphite films are left on Cu grids. Figure 6 shows the bright field TEM micrograph and a corresponding selected area electron diffraction pattern with the electron beam aligned parallel to the [0001] zone axis of the graphite. The streaks which form rings around the six-spot patterns suggest that the graphite consists of turbostratic layers (i.e. a layer with nearly random azimuthal orientation). This finding is similar to the carbon films deposited by pyrolysis or evaporation at high temperature on other crystalline metal substrates.[5,9-13] The neighboring crystals are misoriented to each other about the c-axis. These graphite islands are formed by the out-diffusion process during elevated temperature implantation through the carbon dissolution-precipitation mechanism.[11,14,16] This mechanism relies on the extremely low solubility of C in Cu (0.0001% at 1100 °C)[15] and the fact that copper does not react with carbon to form a carbide because of a filled d-electron shell {$[Ar]3d^{10}4s^1$}.[14] The preferential alignment of the graphite c-axis perpendicular to the substrate is caused by the highly anisotropic nature of graphite lattice and the presence of a flat metal surface.[16] Formation of these highly crystalline films is enhanced by the crystalline nature of the copper substrate.[10]

The result that a graphite film is formed on the surface during elevated temperature implantation is in agreement with the results reported by Lee, et.al.[16], but is contrary to the report by Prins, et . al.[17] that claimed that epitaxial diamond layer was formed directly by the ion implantation technique. In Figure 6, we note that the film develops some cracks, approximately 1000 Å wide, which originate from the difference in the coefficient of thermal expansion between graphite and copper ($\alpha_{a\text{-axis,graphite}} = 0.9 \times 10^{-6}$ /K at 800 °C , c.f. $\alpha_{Cu} = 24 \times 10^{-6}$ /K),[18] causing the graphite film to experience large compressive stress during cooling. The cracks result in the two diffraction spots near the incident beam. They are indexed as the (0002) reflection spots of graphite indicating that the prism planes of graphite at the cracks are almost parallel to the copper crystal surface.

B. Diamond nucleation and growth

Diamond nucleation has been attempted on both pure and carbon implanted Cu. The diamond crystals were grown by MPACVD using 3% CF_4 and 0.7% O_2 in H_2. The diamond crystals obtained on either surface are polycrystalline. No indication of epitaxial growth or growth with preferred orientation has been observed. However, the graphite layer on the Cu surface is found to enhance diamond nucleation quite significantly. This is shown by the optical micrographs in Figure 7. They depict the preferential nucleation of diamond crystals on graphite "dots" formed on the Cu crystal surface by carbon implantation through a Ta shadow mask at 840 °C. They also show that the diamond crystals are preferentially found near the edges of the graphite islands, which can be clearly seen in Fig. 7(b), which is a high-magnification micrograph.. These findings are further supported by the observation of massive nucleation of diamond crystals on

the edges of the graphite cracks, as shown by the many bright spots in the SEM micrograph given in Figure 8(b). This picture was taken on C-implanted Cu after being exposed for 2 minutes in 1% CH_4/H_2 plasma, while Figure 8(a) shows, for a comparison, the surface feature prior to diamond nucleation. This implies that some interesting chemistry is involved in the diamond deposition reactions on graphitic surfaces, which will be discussed later. The Raman spectrum taken from this sample (see Figure 9) confirms the presence of a crystalline diamond phase as indicated by the sharp spectral feature at a wavenumber shift of 1332 cm^{-1}.

Diamond crystals can also grow on carbon-implanted copper crystals at room temperature, but the nucleation density is lower and the crystals are smaller than those grown on substrates implanted at elevated temperature (for similar deposition conditions). It is believed that the size difference is related to the time required for the implanted carbon to diffuse to the surface where it forms a graphite layer. Diamond crystals obtained on this kind of samples were found to be polycrystalline also.

An attempt to nucleate diamond on Cu(111) implanted with carbon at 120 keV, $1x10^{18}$ ion dose, and room temperature conditions yielded no difference in results as the one grown on Cu(111) implanted at 60/75 keVat room temperature. This is shown by the SEM micrographs given in Figure 10, where diamond crystals were grown using 0.5% CH_4, and 0.6% O_2 in 200 sccm H_2 at 33 Torr and 800 °C. The interesting thing about this experiment is that the implanted carbon was embedded far beneath the Cu surface (~1500 Å deep) and only a trace amount of carbon was left on the Cu surface. Prior to diamond growth, the substrate was

exposed to H_2 and O_2 (200 sccm : 0.6 sccm) plasma for about 10 minutes. This was carried out with the hope that there would be ample time for the carbon species to slowly diffuse out to the substrate surface and to form epitaxial diamond phase with the Cu substrate. Apparently, only polycrystalline diamonds with the distinctive twin defects were obtained. Figure 11 shows the Raman spectrum of the diamond crystals. A strong and sharp diamond peak shift at 1332 cm^{-1} wavenumber is clearly observed. The graphite band around 1500 cm^{-1} wavenumber is present also, but is relatively small.

In order to confirm that diamond nucleates and grows on the graphite edges of the planes, we studied the growth of diamond on highly oriented pyrolytic graphite (HOPG) crystals. Similar to what was found previously, diamond crystals were found to nucleate primarily at the edges of the graphite sheet. SEM micrographs in Figure 12 show a striking difference in the diamond nucleation density on the prism plane [Fig. 12(a)] and the basal plane [Fig. 12(b)] of graphite.

Scanning tunneling microscopy experiments were carried out to examine the initial stages of diamond nucleation on the HOPG surfaces. Figure 13 depicts a STM image of a graphite crystal, which had been exposed to 3% CF_4 and 0.7% O_2 in H_2 plasma environment at 33 Torr for one minute. The diamond crystals have started to nucleate, as shown in bright portion in the micrograph. At the center of this image, graphite hexagonal lattices are still visible. Indeed, we find that diamond crystals nucleate right at the edges of the basal plane of graphite crystal. Notice that the STM image was collected in the height mode to prevent the STM tip from crashing upon encountering the diamond grains.

C. Graphite edge chemistry

The phenomenon of the preferential nucleation of diamond near the edges of the graphite lattice shown previously is not surprising when one considers the fact that the fundamental chemistry of the basal and prism (edge) planes of graphite is very different. It is known that the bonding on the basal plane of graphite lattice is saturated with π (sp^2) bonding and the carbon-carbon bond in this plane is very strong. Each carbon in the prism plane, however, has one dangling bond resulting in a lower bond strength. Many previous studies of reactions of graphite with oxygen,[19-26] for example, have shown strong evidence that the carbon-carbon bonds on the edges of the carbon sheets represent the weakest and thus the most reactive sites in the graphite lattice. Grisdale[26] reported an anisotropy factor of 17 for graphite oxidation reactions in the a and c directions, while some other workers[20] quoted a value as high as 25-27. Although the basal plane can also be involved in the reaction[24] and its reactivity may be enhanced by the presence of lattice vacancies[19], the majority of the action still takes place at the prism plane.

Similarly to the case of oxygen reaction, the basal plane surface of graphite is less affected by atomic hydrogen compared to the prism plane surface.[27] An apparent reaction probability of graphite in producing CH_4 or C_2H_2 products by atomic hydrogen was found to be approximately one order magnitude higher on the prism plane than on the basal plane at a given temperature. A sticking coefficient of atomic hydrogen was found to be 0.02 on the prism plane and only 0.006 on the basal plane of graphite. The same study also found that the rate constants of the

reactions for the two planes are comparable in activation energy but much higher in the pre-exponential factor for the prism plane.

We have carried out a study of etching of graphite by atomic hydrogen for different times of exposure. The results, examined by STM and AFM techniques, are given in Figure 14. The atomic STM image of the graphite basal plane surface prior to the etching experiments is shown in Figure 14(a). A perfect hexagonal image of the lattice is clearly resolved. The C-C bond distance is measured to be approximately 1.4 Å, in reasonable agreement with the literature value of 1.42 Å. Deterioration of the lattice by atomic hydrogen starts at a very early stage (i.e. after approximately 1 minute etching) by the creation of many lattice vacancies as predicted earlier.[19,28] This is seen in a STM image in Fig. 14(b). After three minutes of plasma exposure [Fig. 14(c)], the surface of graphite has been so severely roughened that the atomic imaging becomes impossible. Hexagonal etch pits are seen and they become clearer after five minutes of the etching experiment, as given by the AFM image in Figure 14(d). The formation of the etch pits with hexagonal symmetry occurs because of the anisotropic reactivity of carbon along the principal crystallographic orientations on the basal planes (<$10\bar{1}0$> and <$11\bar{2}0$>).

It is, therefore, believed that the initial stage of diamond nucleation on a graphitic surface involves the hydrogenation of the graphite lattice plane edges or the disruption of the graphite basal lattice to create the edges. It should be noted also that reactions involving the direct attachment of CH_n radicals to the graphite basal plane surface are extremely unlikely. The sticking coefficient of CH_n radicals

to an ideal graphite surface is believed to be very small, and is estimated to be ~0.03 or smaller.[29-31] This is supported by the work of Vandentop et al.[32] on the extremely slow initial deposition rate of a-C:H onto the graphite surface. They suggested that a disruption of the graphite surface by high-energy ions is essential for the radicals to be attached chemically to the graphite surface.

In the hydrogenation reaction of graphite, a reaction involving hydrogen insertion at the $\{11\bar{2}L\}$ lattice ("arm-chair") planes, but not the $\{10\bar{1}L\}$ planes ("zig-zag"), of graphite is considered to be the most likely reaction path[23,33] in the temperature range for CVD diamond growth. Schematic diagrams of both elementary mechanisms are given in Figure 15. The likelihood of the occurrence of the "arm-chair"reaction can be explained by two simple arguments. The first argument is based on the electronic structure of the carbon edge atoms on graphite. Coulson's model[34], which is based on the consideration of the unsatisfied nature of the extra electrons at the graphite edge atoms, pointed out the fact that the carbon atoms in the "arm-chair" configuration attain a partial triple bonding character upon pairing the electrons between the two neighboring carbon atoms. This can be formed without significantly affecting the behavior of the resonating electrons in the π bond system. The atoms in the "zig-zag" form, however, tend to be in divalent states based on s^2p^2 hybridization. This type of configuration which allows the two neighboring carbon atoms to form an extra σ bond is energetically more favorable with respect to the original $sp^2\pi$ state. It is more stable and thus less reactive than the triple bond. The second explanation is based on the steric argument. The hydrogenation reaction involving the atoms in the "zig-zag" planes entails a complicated rearrangement of π-electron systems and the steric repulsions,

while no rearrangement in the π-electron systems is necessary to promote the "armchair" reactions.[23]

D. The epitaxial relationship between diamond and carbon-implanted Cu

From the arguments presented in the previous section, it is reasonable to say that a simpler and energetically more favorable way of nucleating diamond on the graphitic surfaces of implanted Cu is by first hydrogenating the carbon atoms at the graphite edge to form sp^3 hybridized CH_3 bonds. This proceeds through the disruption of carbon atoms in the $\{11\bar{2}L\}$ planes. It is then followed by reaction with hydrocarbon radical precursors from the gas phase to form diamond. Figure 16 presents a simple lattice model of a diamond nucleus on the edge of the graphite lattice. According to the proposed model, the {111} plane of diamond is perpendicular to the basal plane of graphite and the $<110>_{diamond}$ is parallel to the $<11\bar{2}0>_{graphite}$. The proposed model is reasonable because the carbon-carbon length in the <110> direction of diamond (2.507 Å) matches that in the $<11\bar{2}0>$ direction of graphite (2.459 Å) within 2 %. In fact, in the high pressure synthesis of diamond from graphite using the explosion shock quenching method, the row of carbon atoms along the $<11\bar{2}0>$ of graphite is believed to transform into the <110> of diamond.[35] The model is also in agreement with the previous study of graphite formation on CVD diamond films in which graphite was found to form with its basal plane matches on or close to the {111} planes of diamond.[36]

IV. CONCLUSIONS

In conclusion, we have made a careful study of the nucleation and growth mechanism for CVD diamond on carbon-implanted single crystal Cu surface. The

surface energy of Cu can be modified by carbon implantation prior to the diamond growth. This process leads to the formation of a turbostratic graphite film on the Cu surface through the out-diffusion process during elevated temperature implantation by the carbon dissolution-precipitation mechanism. Because of the significant difference in coefficient of thermal expansion between graphite and Cu, the graphite films experience a large compressive stress during cooling, resulting in nanometer-wide crackings.

Diamond nucleation has been found to be greatly enhanced on the graphitic surfaces of Cu. In particular, the diamond crystals can preferentially nucleate at the edges of graphite lattice and show no indication of epitaxial growth or growth with preferred orientation in any sample. This result has been further supported by the experiments conducted on HOPG crystals. This phenomenon is explained from the unique chemistry of graphite which shows a strong anisotropic behavior when exposed to atomic hydrogen. From our study we have constructed a simple lattice model for diamond growth on graphitic surface of copper crystals as $<111>_{diamond}$ parallel to $<0001>_{graphite}$ and $<110>_{diamond}$ parallel to $<11\bar{2}0>_{graphite}$. The proposed model is reasonable because the carbon-carbon length in the <110> direction of diamond (2.507 Å) matched that of the $<11\bar{2}0>$ direction of graphite (2.459 Å) to within 2 %. Our results conclude that diamond heteroepitaxy on the carbon-implanted surface of single crystal copper does not occur.

ACKNOWLEDGMENTS

We would like to thank Mr. Mark Seniew for his assistance in growing the single crystal copper. We acknowledge the support of the Office of Naval Research

and DOE Basic Energy Sciences Division (contract NO. DE-FG02-87ER45314). Work carried out at the Oak Ridge National Laboratory was sponsored by the Division of Materials Science, USDOE, under contract DE-AC05-84OR21400 with Martin Marietta Energy Systems, Inc.

REFERENCES

1 M. W. Geis, N. N. Efremow, and D. D. Rathman, J. Vac. Sci. Technol. **A6**, 1953 (1988).

2 H. Nakazawa, Y. Nakazawa, M. Kamo, and K. Osumi, Thin Solid Films **151**, 199 (1987).

3 J. E. Field, in The Properties of Diamond, edited by J. E. Field (New York, Academic Press, 1979), p. 281.

4 D. N. Belton and S. J. Schmieg, J. Appl. Phys. **66**, 4223 (1989).

5 B. C. Banarjee, T. J. Hirth, and P. L. Walker Jr., Nature **192**, 450 (1961).

6 D. L. Trimm, in Pyrolysis : Theory and Industrial Practice, edited by L. F. Albright, B. L. Crynes, and W. H. Corcoran. (New York, Academic Press, 1983), p. 203.

7 S. Koizumi, T. Murakami, T. Inuzuka, and K. Suzuki, Appl. Phys. Lett. **57**, 563 (1990).

8 R. Richter, J. R. Smith, and J. G. Gay, in The Structure of Surfaces, edited by M. A. van Hove and S. Y. Tong (Springer Verlag : New York, 1985), p. 35.

9 P. W. Palmberg, in The Structure and chemistry of Solid Surfaces, edited by G.A. Somorjai. (New York, Wiley, 1969), p. 29.1.

10 A. E. Karu and M. Beer, J. Appl. Phys. **37**, 2179 (1966).

11 F.J. Derbyshire, A.E.B. Presland and D.L. Trimm, Carbon **13**, 111 (1975).

12 A. E. B. Presland and P. L. Walker Jr., Carbon **7**, 1 (1969).

13 S. M. Irving and P. L. Walker Jr., Carbon **5**, 399 (1967).

14 A. Oya and S. Otani, Carbon **17**, 131 (1979).

15 M. B. Bever and C.F. Floe, Trans. AIME **166**, 128 (1946).

16 S. T. Lee, S. Chen, G. Braunstein, X. Feng, I. Bello, and W. M. Lau, Appl. Phys. Lett. **59**, 785 (1991).

17 J. F. Prins and H.L. Gaigher, Proc. 2nd Int. Conf. of New Diamond Science and Technology, edited by R. Messier, J. T. Glass, J. E. Butler, and R. Roy (Materials Research Society : Pittsburgh, 1991), p. 561.

18 J. B. Nelson and D. P. Riley, Proc. Phys. Soc. **57**, 477 (1945).

19 G. R. Hennig, J. Chem. Phys. **40**, 2877 (1964).

20 J. M. Thomas, in Chemistry and Physics of Carbon Vol. 1, edited by P. L. Walker, Jr. (New York: Dekker, 1965), p.121, and references therein.

21 E. L. Evans, R. J. M. Griffiths, and J. M. Thomas, Science **171**, 174 (1971).

22 D. R. Olander, R. Jones, J. A. Schwarz, and W. Siekhaus, J. Chem. Phys. **57**, 421 (1972).

23 A. Tomita and Y. Tamai, J. Chem. Phys. **78**, 2254 (1974).

24 R. T. Yang and C. Wong, J. Chem. Phys. **75**, 4471 (1981).

25 D. W. McKee, in Chemistry and Physics of Carbon Vol. 16, edited by P. L. Walker, Jr. and P. A. Thrower. (New York : Dekker, 1981) p. 1, and references therein.

26 R. O. Grisdale., J. Appl. Phys. **24**, 1082 (1953).

27 M. Balooch and D. R. Olander, J. Chem. Phys. **63**, 4772 (1975).

28 F. S. Feates, Carbon **6**, 949 (1968).

29 G. J. Vandentop, M. Kawasaki, R. M. Nix, I. G. Brown, M. Salmeron, and G. A. Somorjai, Phys. Rev. **B41**, 3200 (1990).

30 L. E. Kline, W. D. Partlow, W. E. Bies, J. Appl. Phys. **65**, 70 (1989).

31 H. Toyoda, H. Kojima, and H. Sugai, Appl. Phys. Lett. **54**, 1507 (1989).

32 G. J. Vandentop, P. A. P. Nascente, M. Kawasaki, D. F. Ogletree, G. A. Somorjai, and M. Salmeron, J. Vac. Sci. Technol. **A9**, 2273 (1991).

33 C. W. Zielke and E. Gorin, Ind. Eng. Chem. **47**, 820 (1955).

34 C. A. Coulson, Proc. of the 4th Conf. on Carbon. (New York : Pergamon Press, 1960), p. 215.

35 E. J. Wheeler and D. Lewis, Mat. Res. Bull. **10**, 687 (1975).

36 W. Zhu, C. A. Randall, A. R. Badzian, and R. Messier, J. Vac. Sci. Technol. **A7**, 2315 (1989).

LIST OF FIGURE CAPTIONS

FIG. 1. 2.45 GHz microwave plasma CVD apparatus for growing diamond films.

FIG. 2. Optical micrograph of a carbon layer implanted into Cu(100) surface at 820 ^{o}C, 1 x10^{18} dose, and 70 keV.

FIG. 3. RBS and ion channeling spectra of virgin and carbon implanted Cu(100). The conditions of the implantation are : 820 ^{o}C, 1x10^{18} ions/cm^2 dose, and 70 keV.

FIG. 4. RBS and ion channeling spectra of virgin and carbon implanted Cu(100). The conditions of the implantation are : room temperature, 1 x10^{18} ions/cm^2 dose, and 70 keV.

FIG. 5. X-ray diffraction of carbon implanted Cu(111). The copper signal is obtained by the normal $\theta/2\theta$ scan using 20 kV and 5 mA X-ray Cu K_α line. For the case of carbon signal, the θ scan is carried out using 40 kV and 20 mA.

FIG. 6. (a) A plan view TEM micrograph (bright field) of a carbon layer formed by carbon ion implantation into Cu(111) at elevated temperature; (b) a corresponding select area electron diffraction patter of the carbon layer.

FIG. 7. Optical micrographs (a) low magnification , (b) high magnification. showing preferential nucleation of diamond crystals on the edges of graphite islands on Cu(111). The circle patch of the graphitic islands were formed by C implantation through a Ta shadow mask at the following conditions : 75 keV, 1x10^{18} ions/cm^2 dose, and 840 ^{o}C.

FIG. 8. SEM micrographs of 820 ^{o}C C-implanted Cu surfaces:(a) before and (b) after 1% CH_4/H_2 plasma treatment.

FIG. 9. Raman spectrum of diamond crystals grown on Cu (111) implanted with carbon at 820 °C. The diamond deposition conditions are : 3% CF_4, 0.7% O_2 in 200 sccm H_2 at 33 Torr and 800 °C. The spectrum was collected using 488 nm Ar laser line.

FIG. 10. SEM micrographs of diamond crystals grown on Cu(111) implanted with carbon at 120 keV, $1x10^{18}$ ion dose, and 820 °C. (0.5% CH_4, 0.6% O_2 in 200 sccm H_2 at 33 Torr and 800 °C).

FIG. 11. The Raman spectrum of diamond particles shown in FIG. 10.

FIG. 12. SEM micrographs showing the distinct difference in diamond nucleation density on the (a) prism ; and (b) basal planes of HOPG crystals.

FIG. 13. STM microscope image of basal plane of perfect graphite lattice near the edge of a step after 1 min diamond growth in 3% CF_4, 0.7 % O_2 and H_2 plasma environment at 33 Torr and 800 °C.

FIG. 14. Results of atomic hydrogen etching of HOPG crystals in microwave plasma (H_2 : 20 sccm ; He : 20 sccm ; power : 100 W ; 10 Torr ; 100 - 400 °C):(a) STM image before etching ; (b) STM image after 1 min. etching (b) STM image after 3 min. etching ; (d) AFM image after 5 min. etching.

FIG. 15. The elementary mechanism for the hydrogenation of graphite via the attack of the atoms on the : (a) $\{11\bar{2}L\}$ plane ("arm-chair") ; (b) $\{10\bar{1}L\}$ plane ("zig-zag").[23]

FIG. 16. A simple model of diamond nucleus on the edge of graphite basal plane where <111>diamond // <0001>graphite and <110>diamond // $<11\bar{2}0>$graphite.

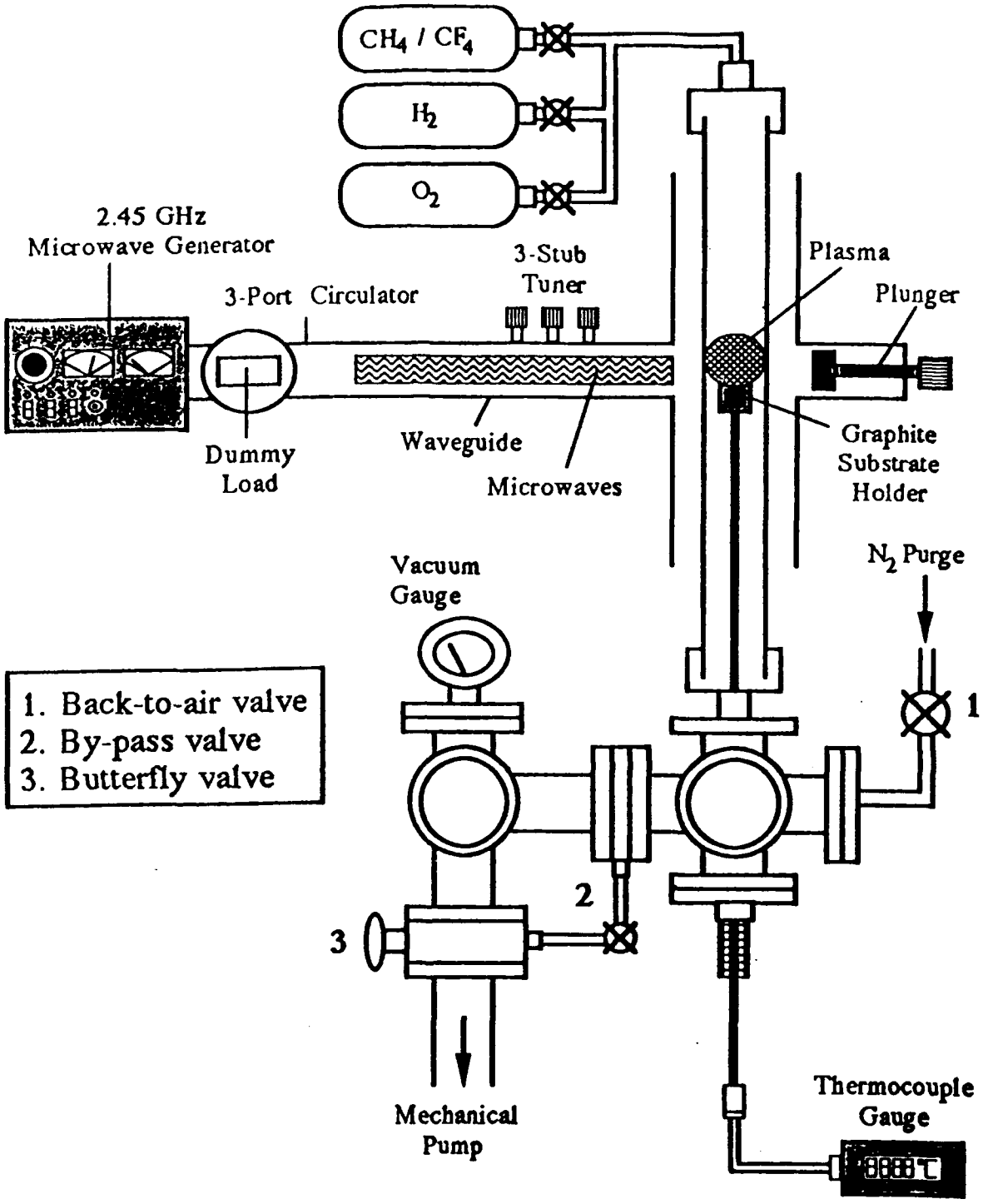
CH_4 / CF_4
H_2
O_2
2.45 GHz
Microwave Generator
3-Port Circulator
3-Stub
Tuner
Plasma
Plunger
Dummy
Load
Waveguide
Microwaves
Graphite
Substrate
Holder
N_2 Purge
Vacuum
Gauge
1. Back-to-air valve
2. By-pass valve
3. Butterfly valve
1
2
3
Mechanical
Pump
Thermocouple
Gauge

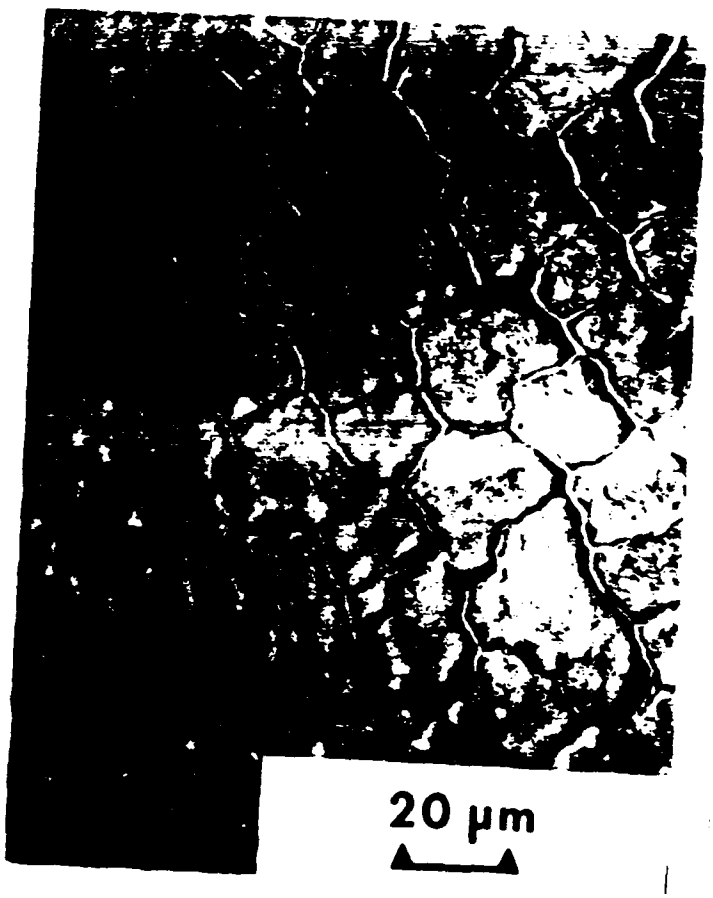
20 µm

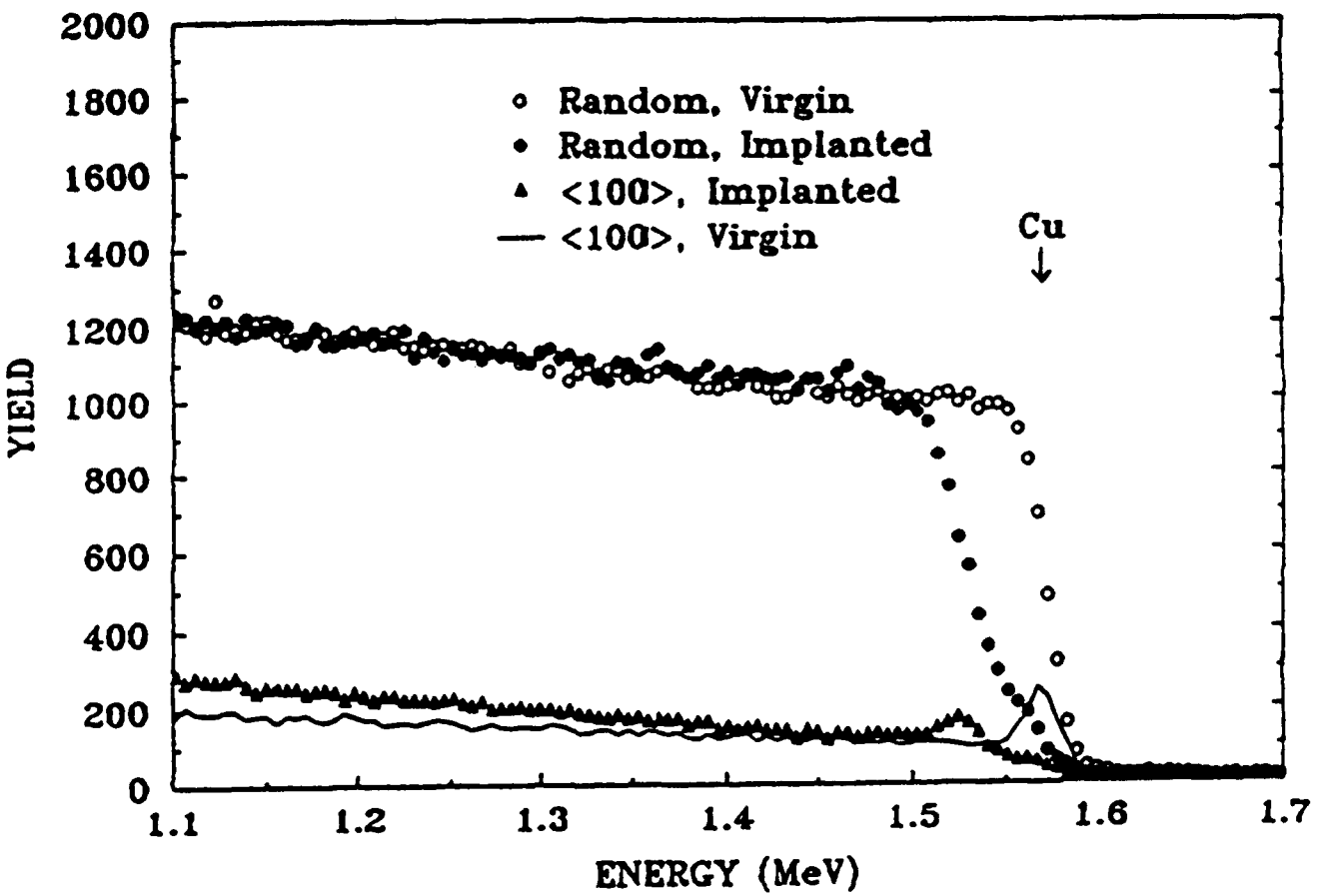
2000
1800
1600
1400
1200
1000
800
600
400
200
0
YIELD
1.1
1.2
1.3
1.4
1.5
1.6
1.7
ENERGY (MeV)
Random, Virgin
Random, Implanted
<100>, Implanted
<100>, Virgin
Cu

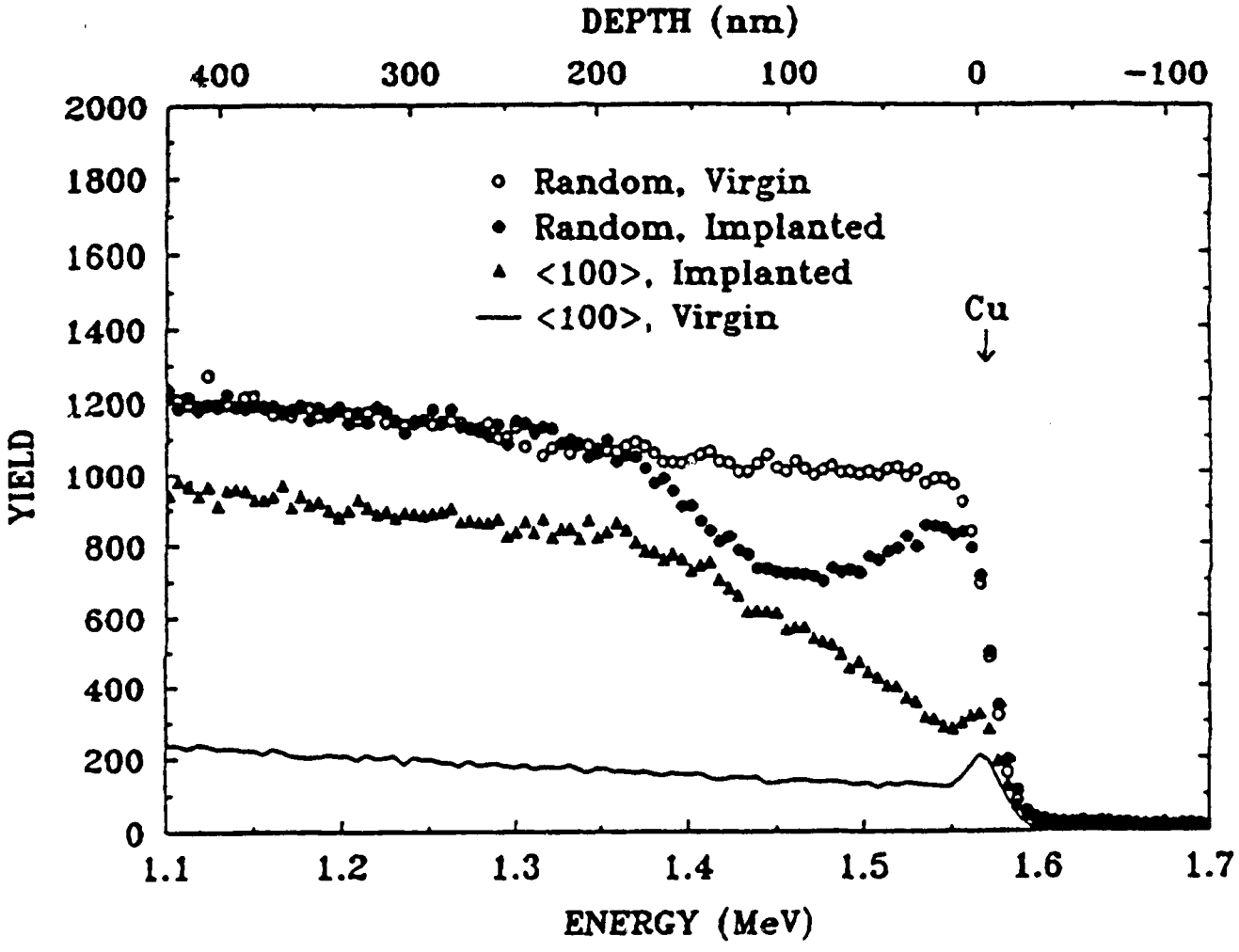
DEPTH (nm)
400
300
200
100
0
−100
2000
1800
1600
1400
1200
1000
800
600
400
200
0
YIELD
Random, Virgin
Random, Implanted
<100>, Implanted
<100>, Virgin
Cu
1.1
1.2
1.3
1.4
1.5
1.6
1.7
ENERGY (MeV)

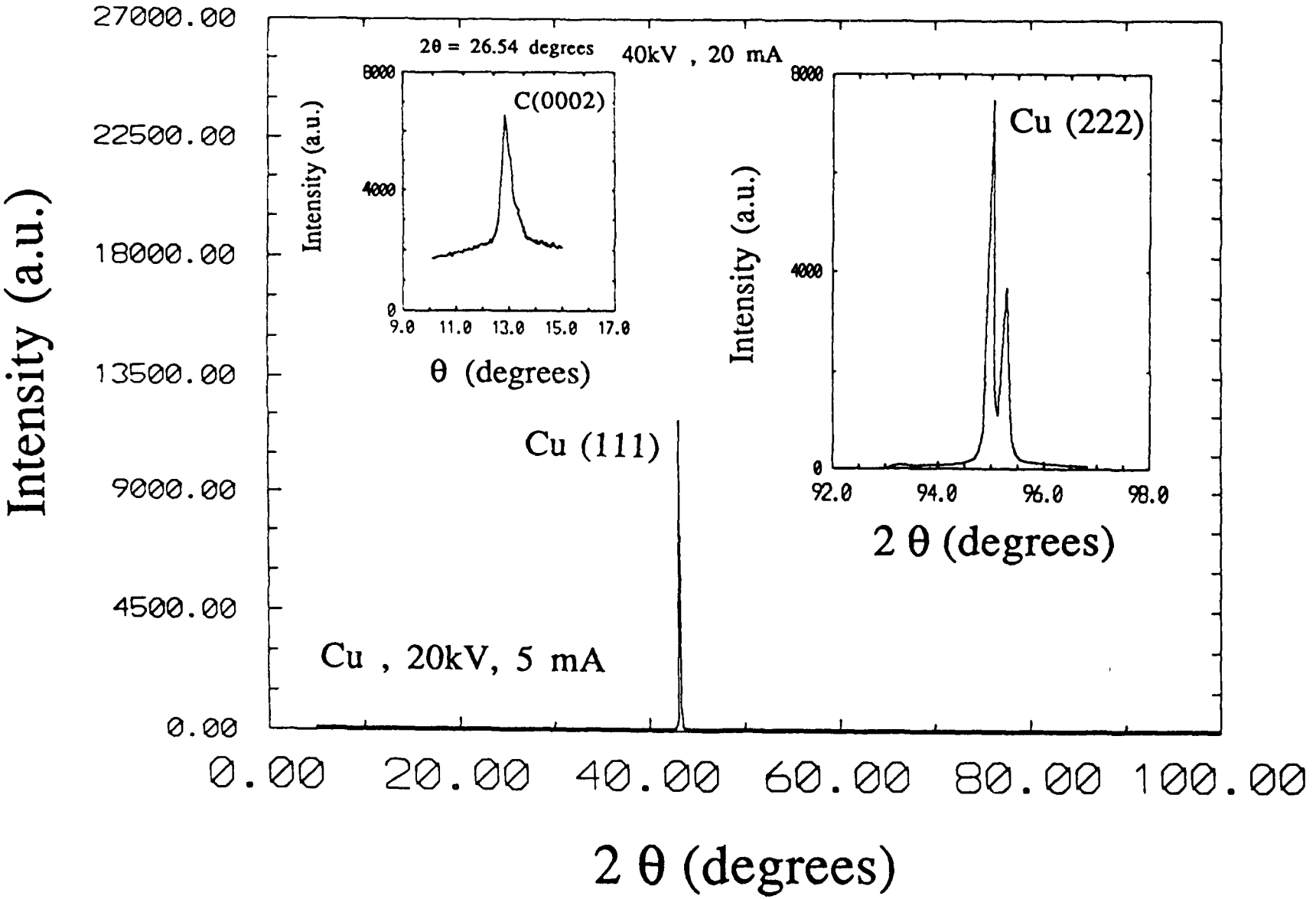
Intensity (a.u.)
27000.00
22500.00
18000.00
13500.00
9000.00
4500.00
0.00
0.00
20.00
40.00
60.00
80.00
100.00
2 θ (degrees)
Cu , 20kV, 5 mA
Cu (111)
2θ = 26.54 degrees
40kV , 20 mA
C(0002)
Intensity (a.u.)
8000
4000
0
9.0
11.0
13.0
15.0
17.0
θ (degrees)
Cu (222)
Intensity (a.u.)
8000
4000
0
92.0
94.0
96.0
98.0
2 θ (degrees)

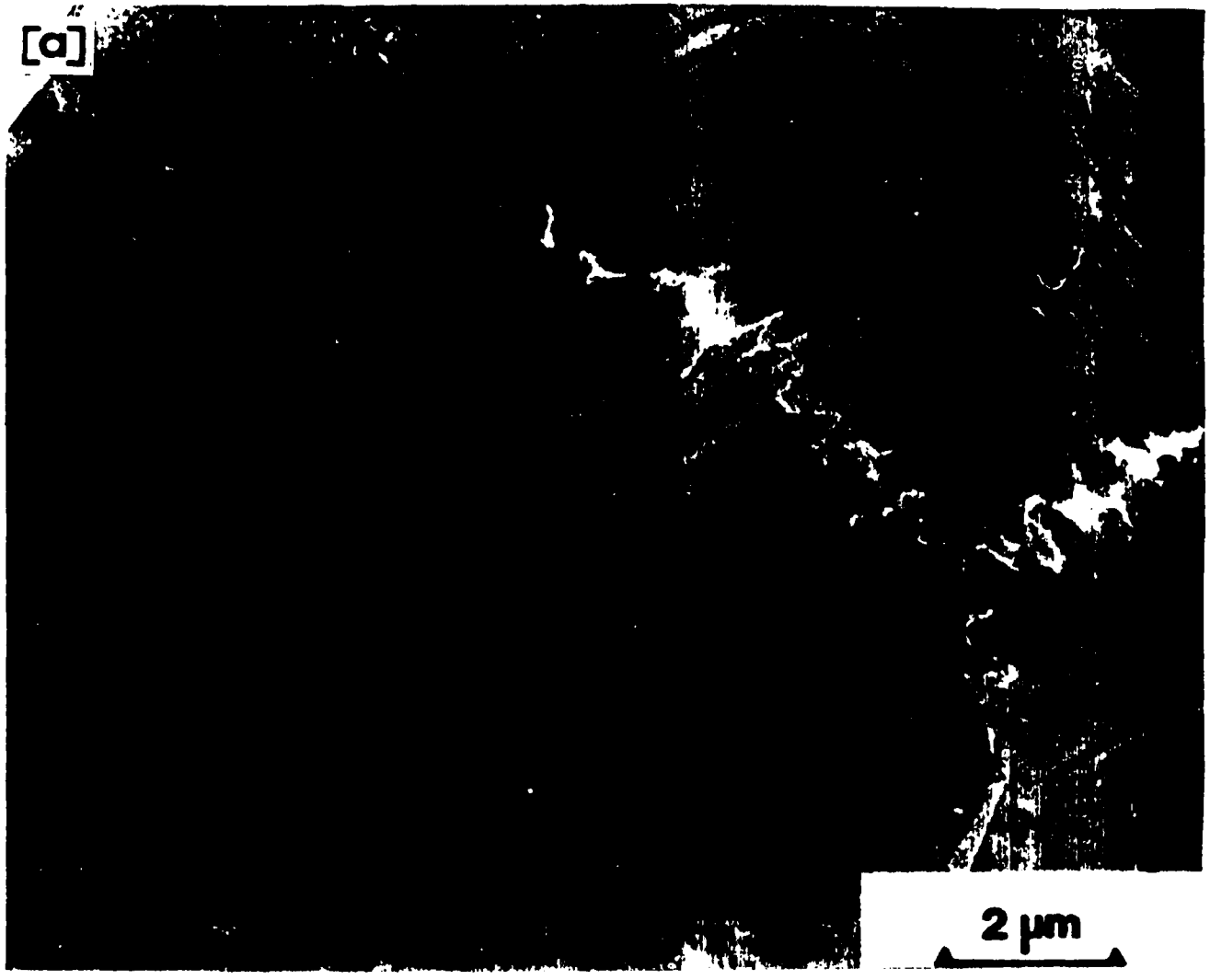
[a]
2 µm

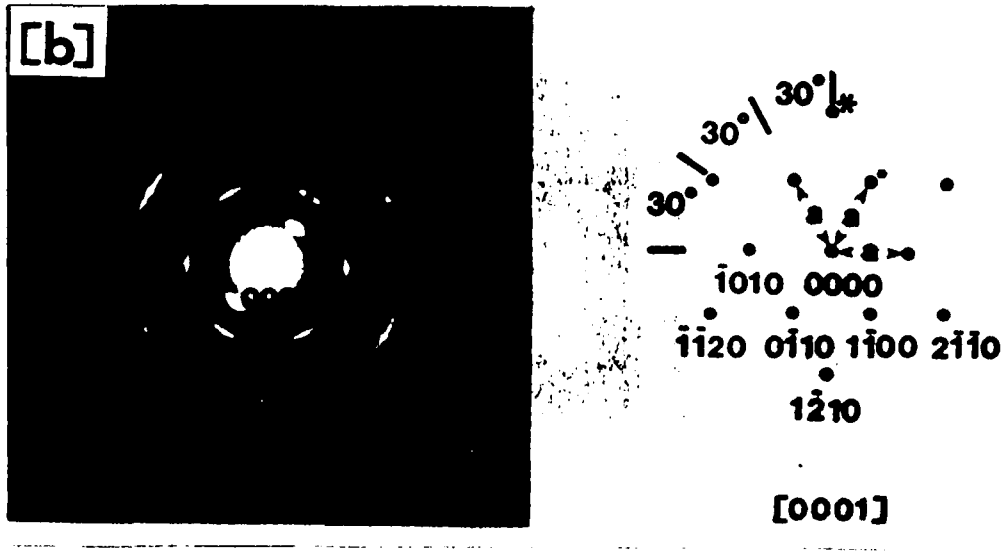
[b]
30°
30°
30°
$\bar{1}010$ 0000
$\bar{1}\bar{1}20$ $0\bar{1}10$ $1\bar{1}00$ $2\bar{1}\bar{1}0$
$1\bar{2}10$
[0001]

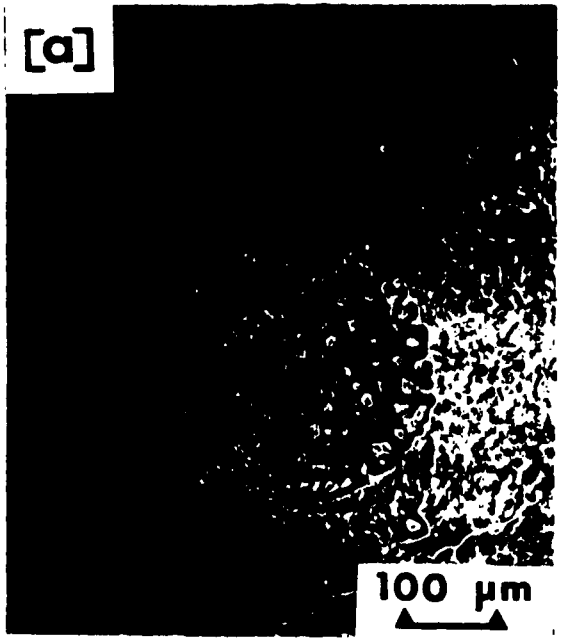
[a]
100 µm

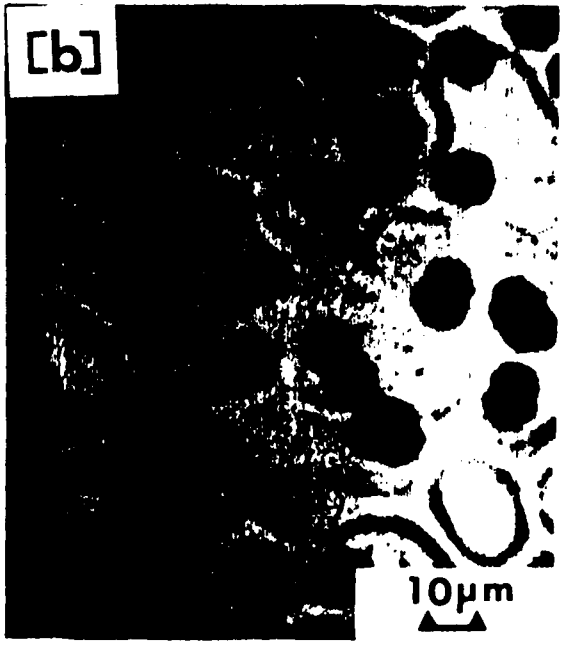
[b]
10µm

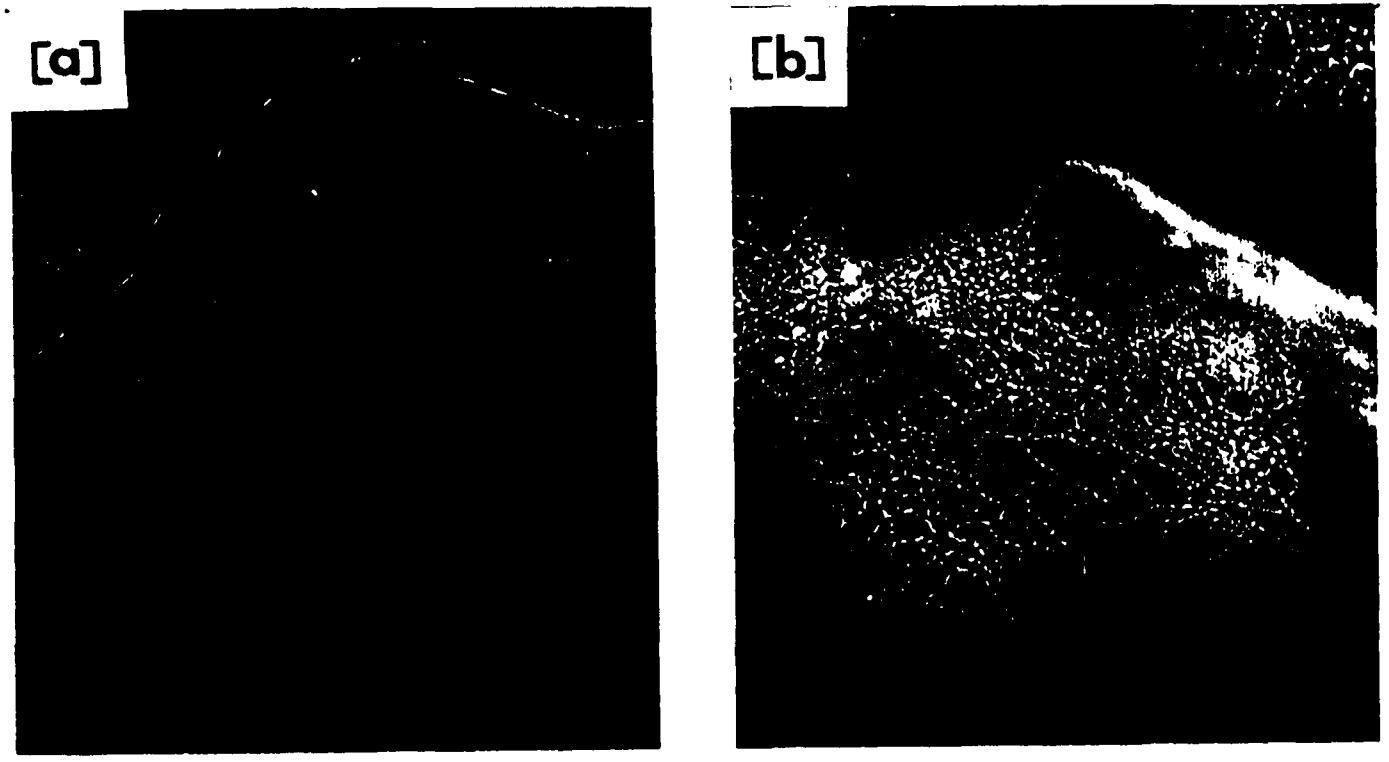
[a]
[b]
2 μm

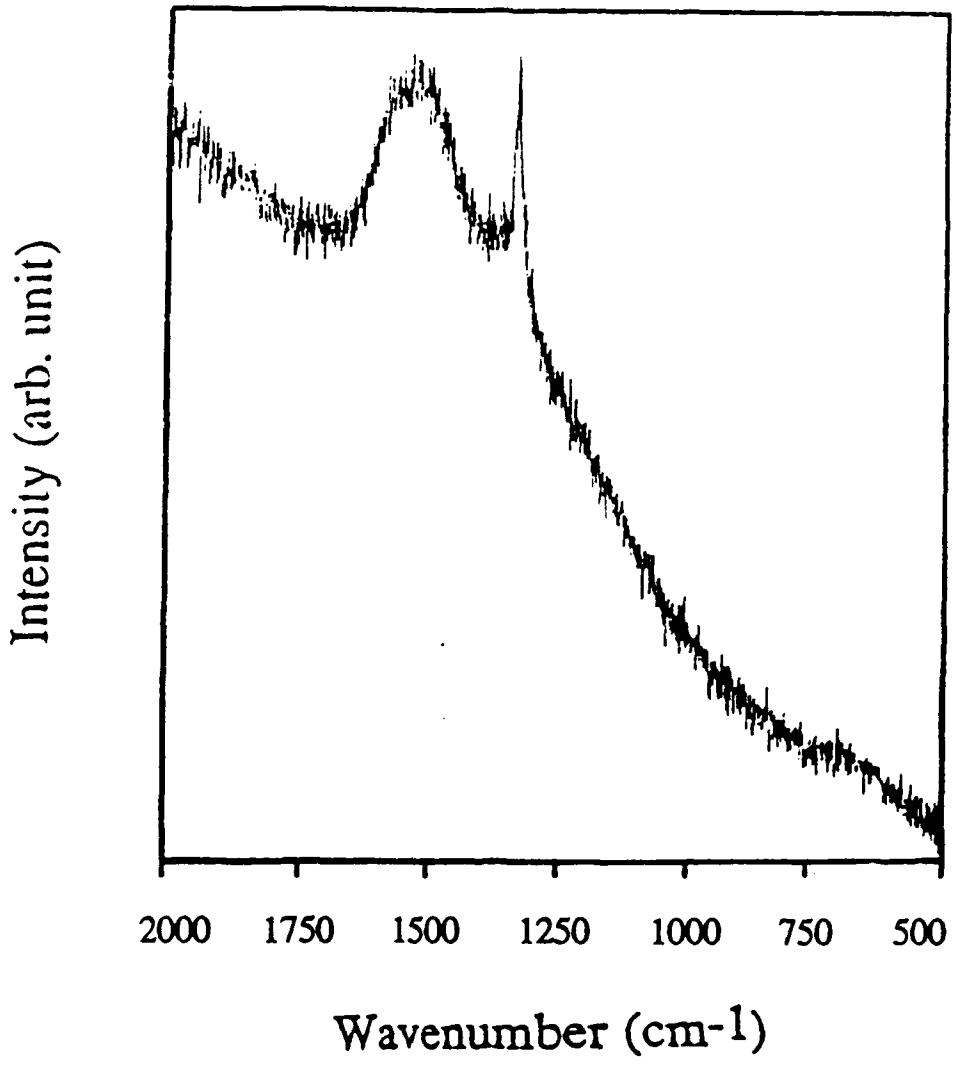
Intensity (arb. unit)
2000
1750
1500
1250
1000
750
500
Wavenumber (cm-1)

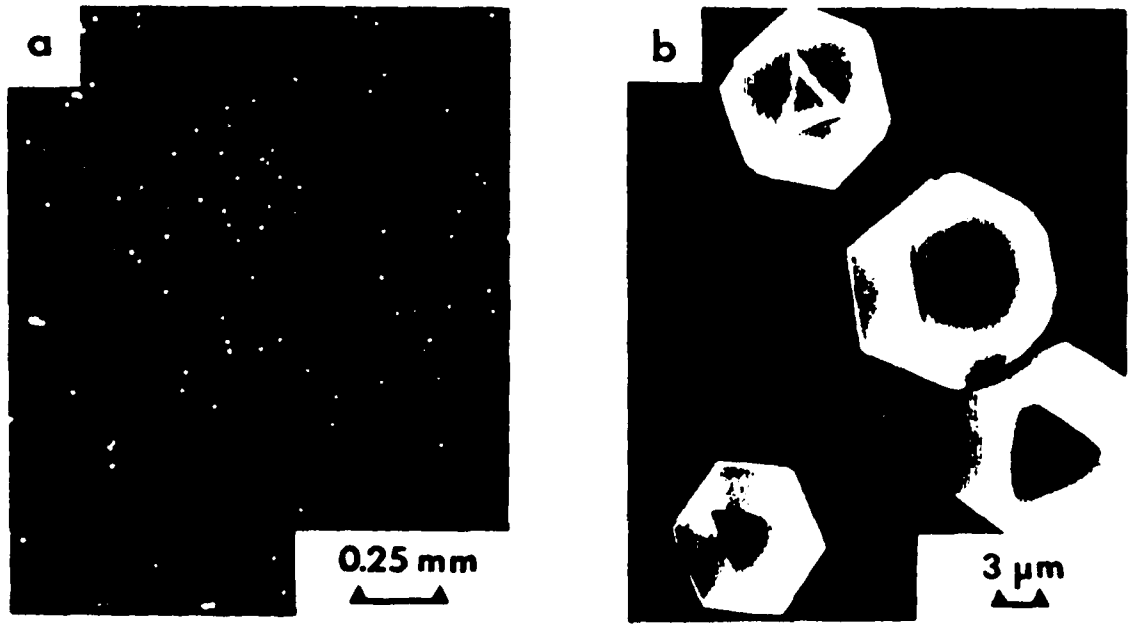
a
0.25 mm
b
3 μm

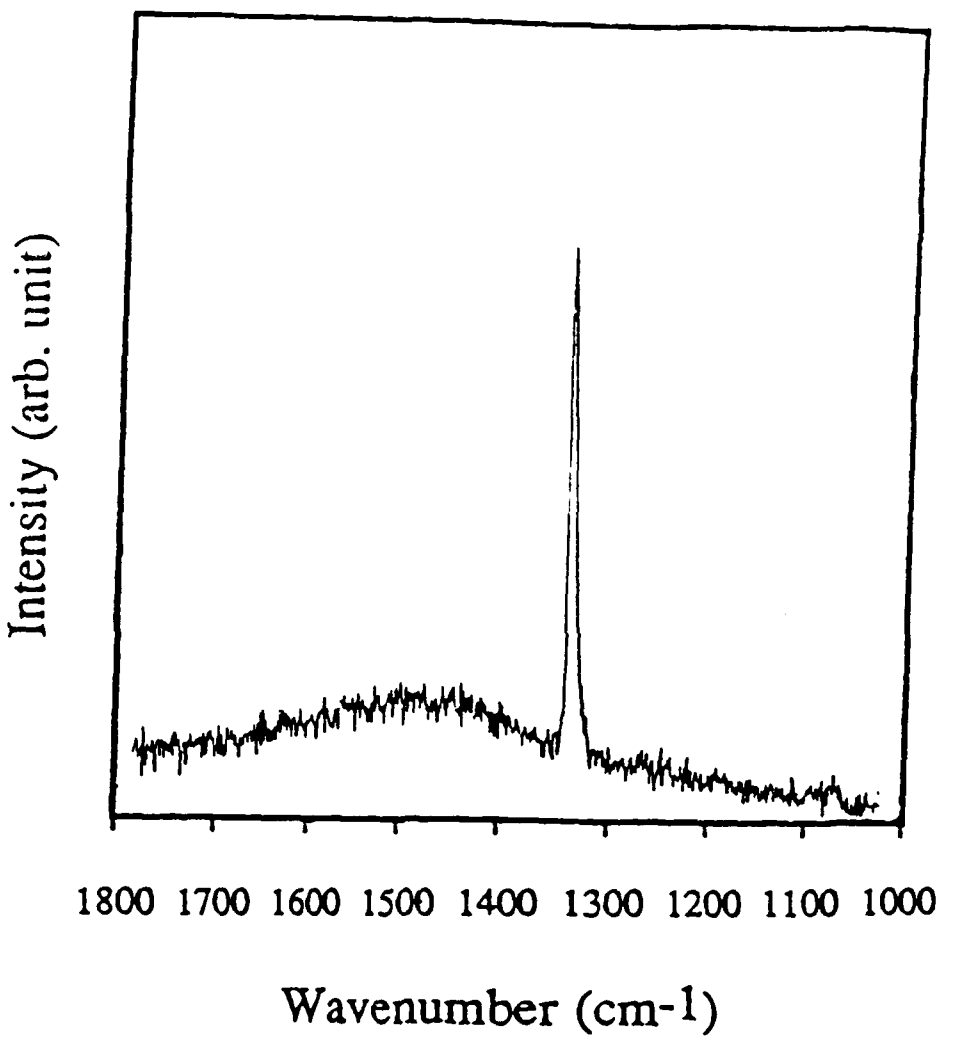
Intensity (arb. unit)
1800 1700 1600 1500 1400 1300 1200 1100 1000
Wavenumber (cm-1)

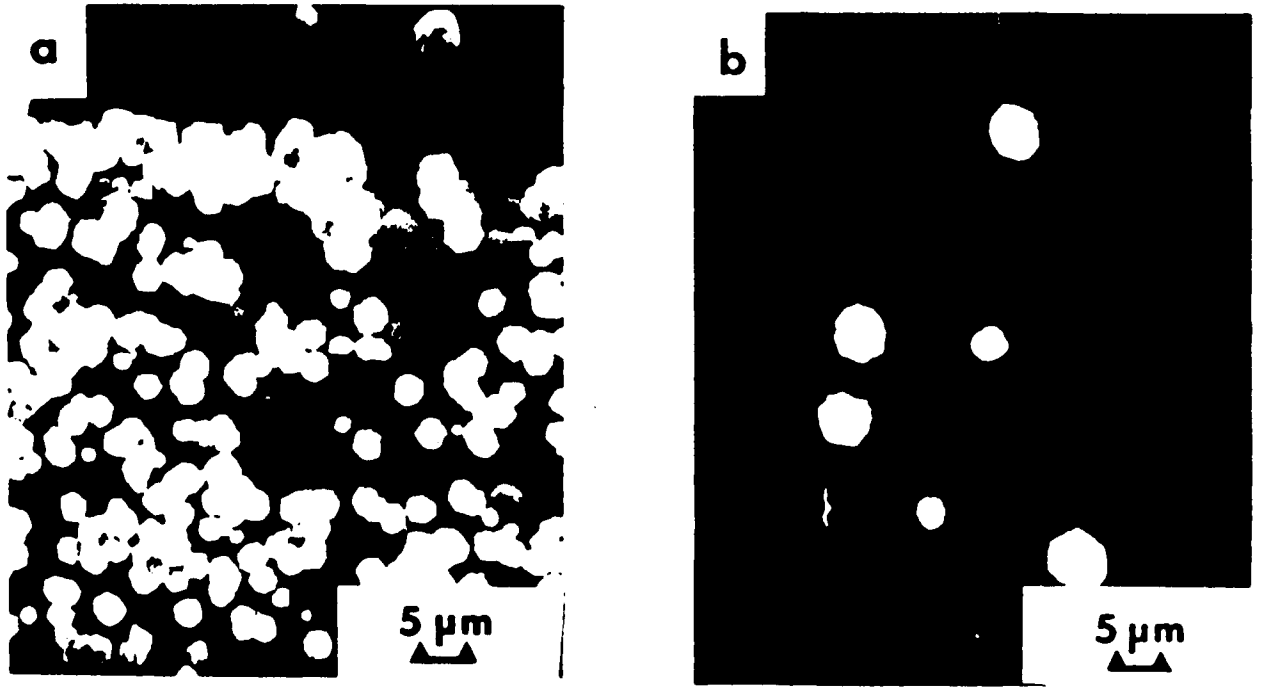
a
5 µm
b
5 µm

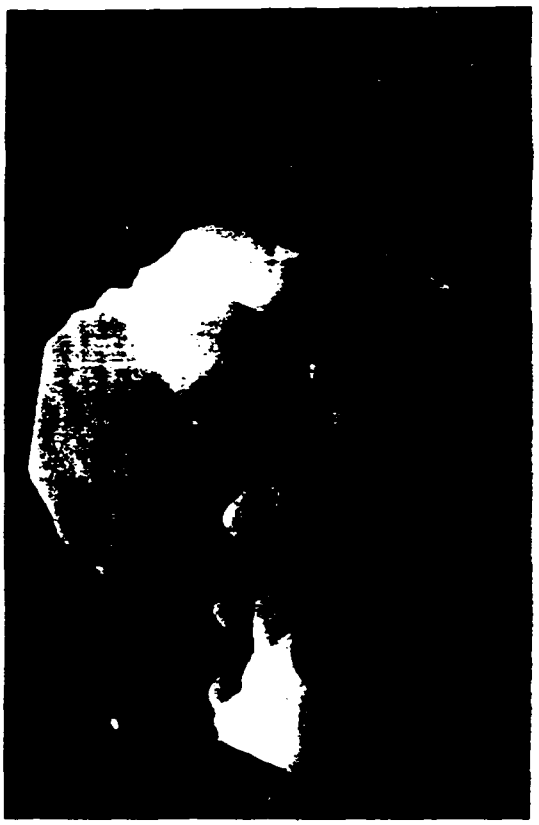

a
b
c
d

(a)

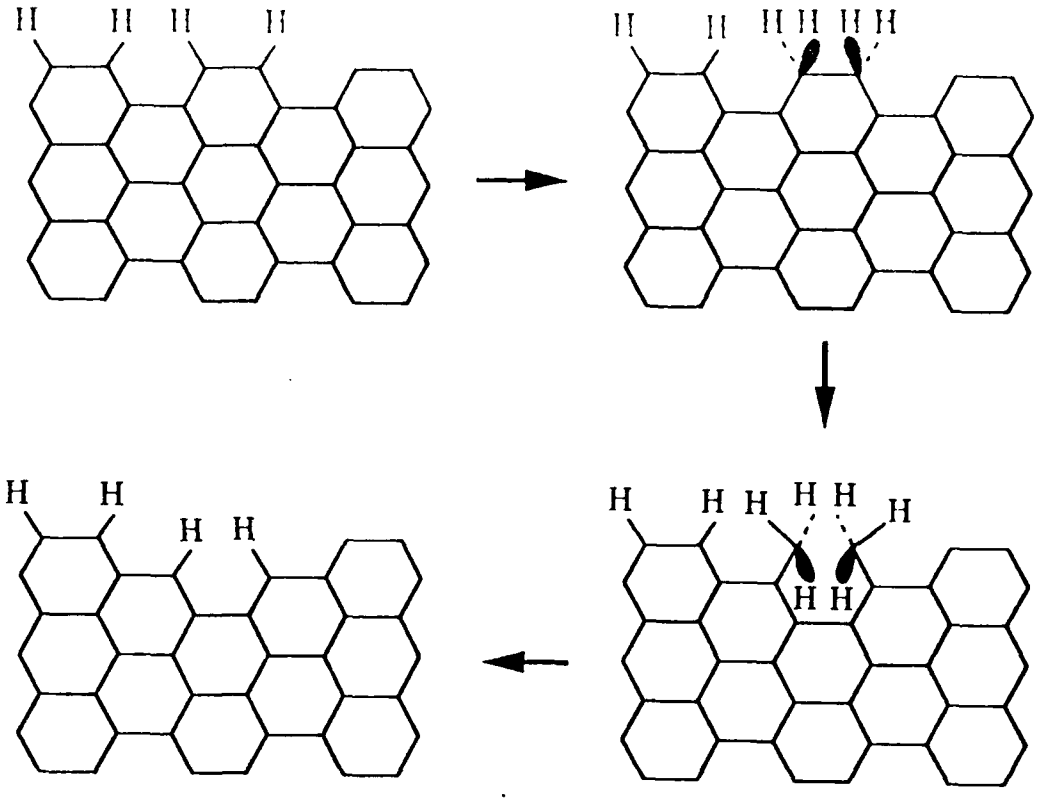

(b)

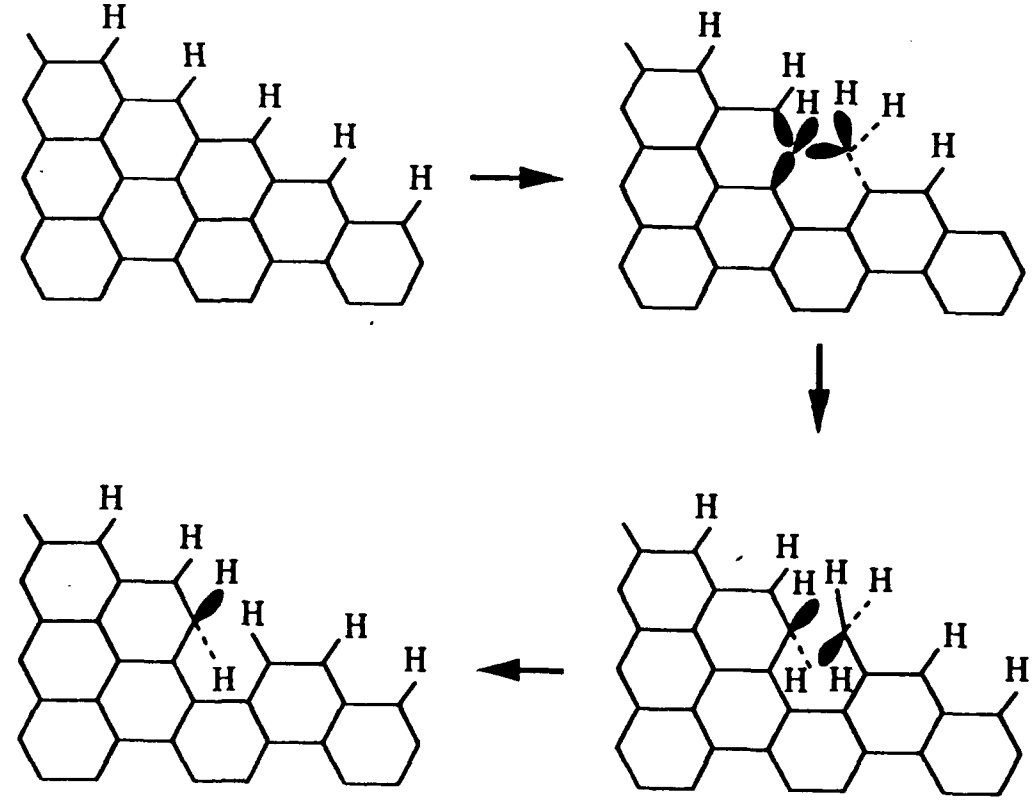

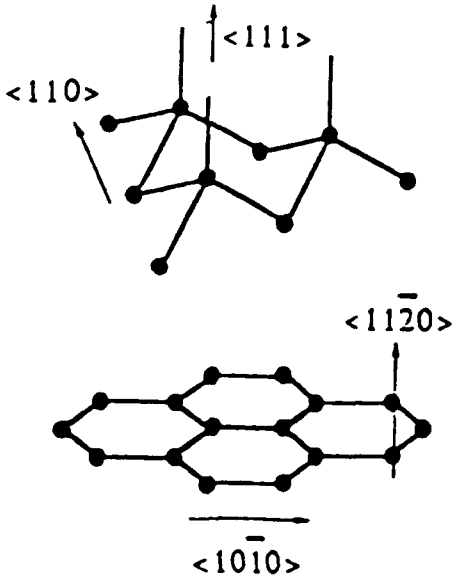
<111>
<110>
<11$\bar{2}$0>
<10$\bar{1}$0>

TECHNICAL REPORT DISTRIBUTION LIST - GENERAL

Office of Naval Research (2)*
Chemistry Division, Code 1113
800 North Quincy Street
Arlington, Virginia 22217-5000

Dr. James S. Murday (1)
Chemistry Division, Code 6100
Naval Research Laboratory
Washington, D.C. 20375-5000

Dr. Robert Green, Director (1)
Chemistry Division, Code 385
Naval Air Weapons Center
Weapons Division
China Lake, CA 93555-6001

Dr. Elek Lindner (1)
Naval Command, Control and Ocean
Surveillance Center
RDT&E Division
San Diego, CA 92152-5000

Dr. Bernard E. Douda (1)
Crane Division
Naval Surface Warfare Center
Crane, Indiana 47522-5000

Dr. Richard W. Drisko (1)
Naval Civil Engineering
Laboratory
Code L52
Port Hueneme, CA 93043

Dr. Harold H. Singerman (1)
Naval Surface Warfare Center
Carderock Division Detachment
Annapolis, MD 21402-1198

Dr. Eugene C. Fischer (1)
Code 2840
Naval Surface Warfare Center
Carderock Division Detachment
Annapolis, MD 21402-1198

Defense Technical Information
Center (2)
Building 5, Cameron Station
Alexandria, VA 22314

* Number of copies to forward